†Electronic Supplementary Information

Nanomanufacturing of High-Performance Hollow Fiber Nanofiltration Membranes by Coating Uniform Block Polymer Films from Solution

Yizhou Zhang,[a] Ryan A. Mulvenna,[b] Bryan W. Boudouris,[b,c] and William A. Phillip[a,*]

[a] Department of Chemical and Biomolecular Engineering, University of Notre Dame, Notre Dame, Indiana 46556, United States. E-mail: wphillip@nd.edu

[b] Charles D. Davidson School of Chemical Engineering and [c] Department of Chemistry, Purdue University, West Lafayette, Indiana 47907, United States.

This supplementary information contains additional SEM micrographs, detailed material synthesis procedure, detailed hollow fiber membrane copper uptake experimental procedures and sample UV-vis absorption spectra, surface pore size statistics and FT-IR spectra for hydrolysis reaction characterization.

1. The Resistance to Flow from Each Layer of the Composite Hollow Fiber Membrane

The resistance to flow contributed by each layer of the composite membrane to the overall resistance can be quantified by using a two resistances (in series) model. This model utilizes the following expression.

$$\frac{1}{Lp_{,composite}} = \frac{1}{Lp_{,PVDF}} + \frac{1}{Lp_{,self-assembled}}$$

Here, $L_{p,i}$ is the permeability of component *i*. The PVDF support membrane had a hydraulic permeability of 240 L m^{-2} h^{-1} bar^{-1}. For the greatest measured permeability of the composite membrane, 27 L m^{-2} h^{-1} bar^{-1}, the resistance contributed by the PVDF support is less than 12% of the overall resistance. For the smallest measured permeability of the composite membrane, 0.6 L m^{-2} h^{-1} bar^{-1}, the PVDF membrane contributes less than 1% to the overall resistance to flow. As such, it is assumed that the PVDF supports did not greatly impact the overall transport performance of the membrane, and their role is only as structural reinforcement for the self-assembled block polymer active layer.

2. Nanofiltration Membrane Permeability Predicted by Hagen-Poiseuille Equation

The Hagen-Poiseuille equation was used to relate the hydraulic permeability (L_P) of the composite membrane to its nanostructural features, namely, the active layer thickness (l), the effective pore diameter (d_P) and the number of surface pores per unit area (N) of the membrane. From the solute rejection analysis, the PI-PS-PDMA-75 hollow fiber membrane had a d_P = 5.1 nm. From the SEM micrograph analysis, a PI-PS-PDMA-75 hollow fiber membrane fabricated with a speed of 2.5 mm s^{-1} and 25 s evaporation time had a porosity of 1.6×10^{14} pores m^{-2}. Using a 40 nm-thick active layer, the hydraulic permeability of a membrane calculated from Hagen-Poiseuille equation is the following.

$$L_P = N\frac{\pi d_p^4}{128\mu l} = 1.6\times10^{14}\frac{1}{m^2}\cdot 3.14\times(5.1\times10^{-9}\,m)^4\cdot\frac{1}{128}\cdot\frac{1}{8.9\times10^{-4}Pa\cdot s}\cdot\frac{1}{40\times10^{-9}\,m}$$

$$\cdot\frac{1\times10^5 Pa}{Bar}\cdot\frac{3600s}{1h}\cdot\frac{1000\,L}{m^3} = 27\,\frac{L}{m^2\,h\,bar}$$

3. Cross-sectional Images of Self-assembled PI-PS-PDMA Membranes with a 40 nm-thick Top Layer

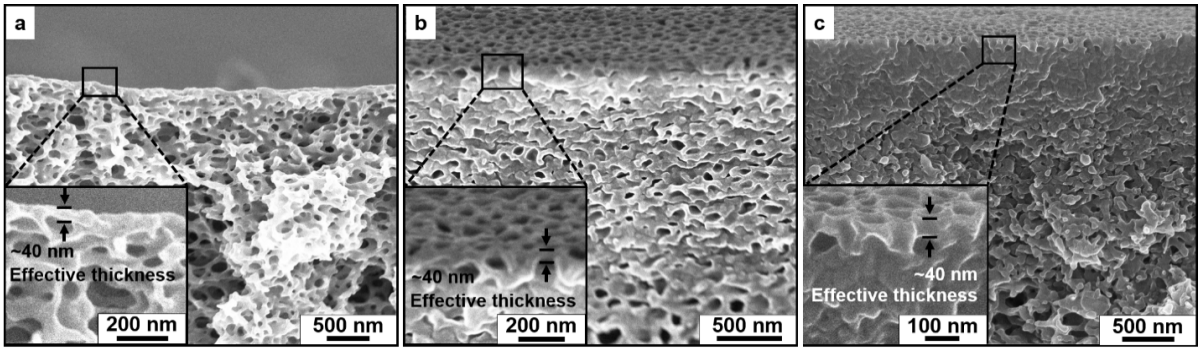

Figure S1. Cross-sectional SEM micrographs for the PI-PS-PDMA membranes at higher magnifications. (a) The PI-PS-PDMA-107 flat-sheet membrane had an asymmetric porous structure. A ~40 nm-thick self-assembled layer was located on top of the membrane. (b) The PI-PS-PDMA-107 hollow fiber membrane had a spongy cross-section. On top of the spongy cross-section is a self-assembled layer where the selecitve layer thickness is approximted as 40 nm. (c) The PI-PS-PDMA-75 hollow fiber membrane, which is fabricated from a 4% (by weight) polymer solution with 5 mm s^{-1} dip-coating speed and 25 s evaporation period, had an asymmetric structure. It also had an self-assembled layer with ~40 nm thickness. The thickness of the self-assembled layer was assumed as the effective thickness of the membrane active layer in the calculation of the hydraulic permeabilities discussed above.

4. Cross-section of a PI-PS-PDMA-107 Membrane Cast on a Glass Slide

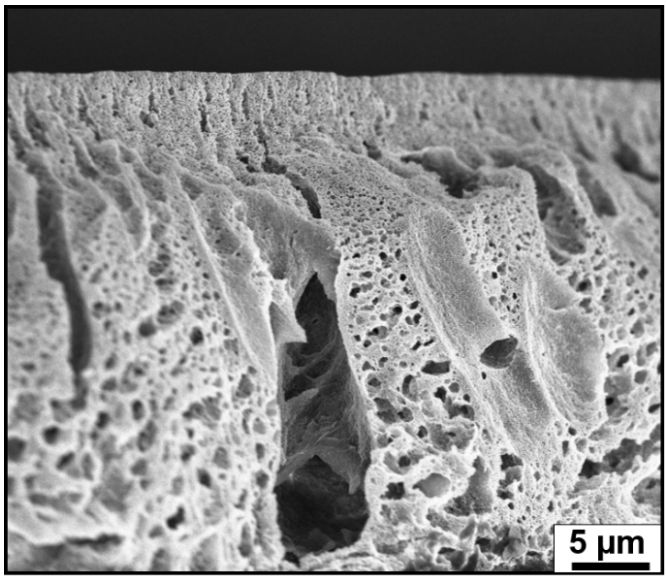

Figure S2. A cross-sectional SEM micrograph of PI-PS-PDMA-107 cast on a glass slide shows the membrane has a ~5 µm active layer and a macroporous supporting layer. The membrane was cast from a 9% (by weight) PI-PS-PDMA-107 polymer solution, which is prepared by dissolving the polymer in a 70/30 (w/w) 1,4-dioxane and tetrahydrofuran solvent mixture.

5. Surface Pore Statistics for two PI-PS-PDMA-107 Membranes Prepared from the Same SNIPS Condition on Different Casting Supports

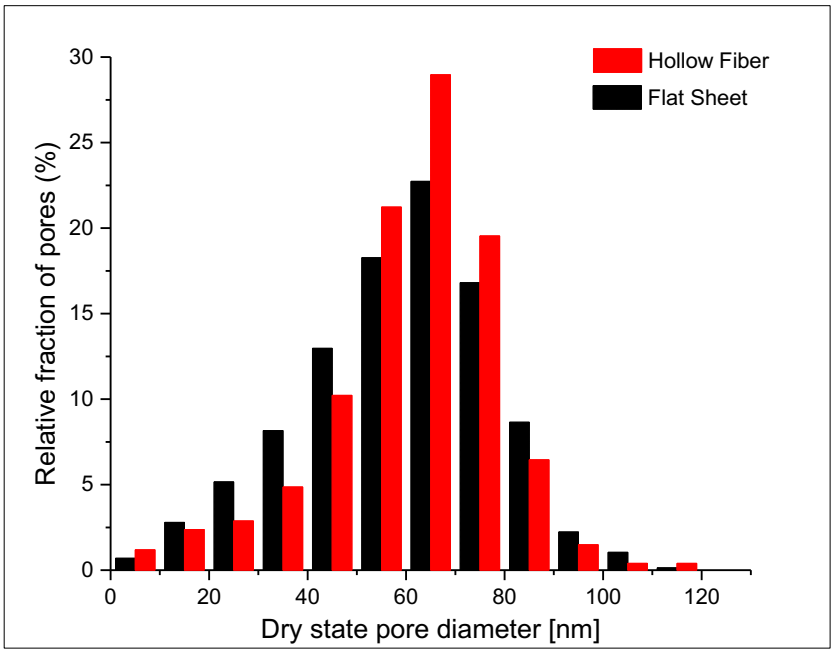

Figure S3. Surface pore statistics, as determined using the ImageJ software package. Two PI-PS-PDMA-107 membranes were prepared from the same SNIPS casting condition but using different casting supports. The flat-sheet membrane had a dry-state pore diameter 60 ± 21 nm, with a porosity of 8.7×10^{13} pores m^{-2}. The hollow fiber had a dry-state pore diameter 61 ± 19 nm and a porosity of 9.2×10^{13} pores m^{-2}. Both the flat-sheet and hollow fiber-supported membranes show a similar porosity and averaged dry-state pore diameter that is ~60 nm. Each bar corresponds to fraction of pores having a specific pore size within 5 nm range. This value fraction was calculated by dividing number of pores having a specific pore size within 5 nm range by the total number of pores imaged on the membrane surface.

6. ATR-FTIR Spectra Confirm the Hydrolysis of PI-PS-PDMA Hollow Fiber Membrane into PI-PS-PAA

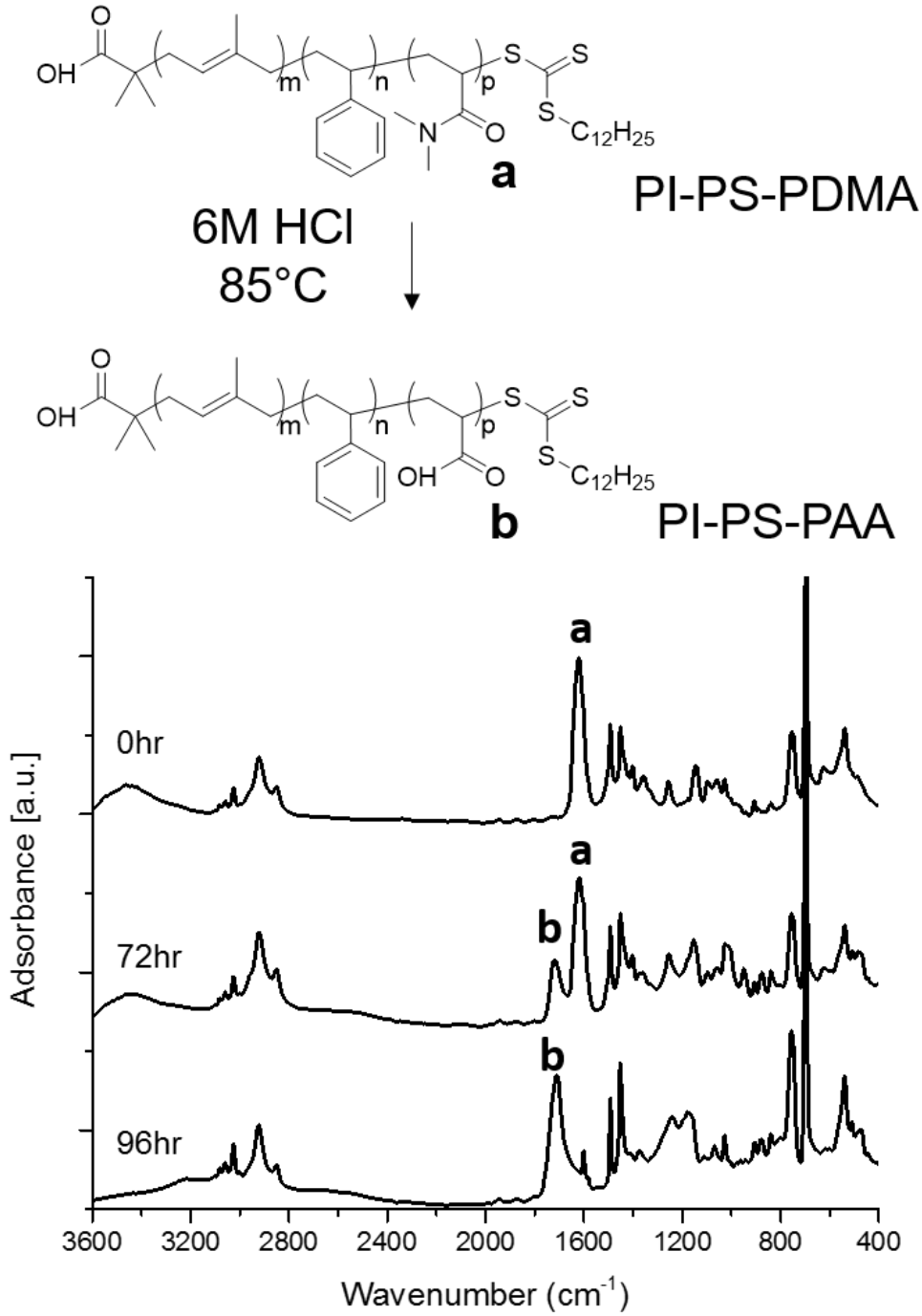

Figure S4. An ATR-FTIR spectrometer was used to monitor the solid state conversion of a PI-PS-PDMA hollow fiber membrane into the PI-PS-PAA membrane. The membrane was placed in an aqueous solution of 6M HCl at 85 ºC for 4 days to reach a full conversion. The membrane was then rinsed with DI water and dried in a vacuum oven for 12 h prior to the analysis. The disappearance of the amide carbonyl group located at ~1600 cm^{-1} (labeled as a) was accompanied by the growth of the carbonyl peak of the carboxylic acid at ~ 1700 cm^{-1} (labeled as b).

7. PI-PS-PAA Hollow Fiber Membrane Captures Copper

The composite PI-PS-PAA hollow fiber membrane was examined as a copper ion adsorber. The copper binding capacity of the membrane was determined using static binding experiments in a manner similar to that described in our previous work.[1] Hollow fiber membranes, segmented into small pieces, were rinsed with DI water, dried under vacuum, and soaked in copper chloride solution overnight with concentration ranging from 1 to 125 mM. The concentrations of copper ion retentate samples were calculated by applying Beer's Law with the maximum in absorbance for the copper ions observed using an ultraviolet-visible (UV-Vis) spectrophotometer at a wavelength of λ = 830 nm. As shown in Figure S5, the vertical shift regarding the maximum peak of adsorption spectra at λ ~830 nm evidenced the decrease in copper ion concentration of a 10 mM copper chloride sample after prolonged soaking.

In order to evaluate the saturation binding capacity, the equilibrium binding capacity was plotted as a function of retentate copper concentration in Figure S5 for solutions ranging in concentration from 1 mM to 120 mM. The equilibrium binding capacity increased with increasing retentate copper ion concentration. The capacity increased sharply from ~1 to 40 mM, and it then began to approach saturation when the retentate concentration was greater than ~ 80 mM. Experimental data were fit into a Langmuir isotherm model. As such, the maximum binding capacity of dual-layer hollow fiber membrane is estimated as 0.60 ± 0.6 mmol g^{-1}, based on the total mass of the composite membrane.

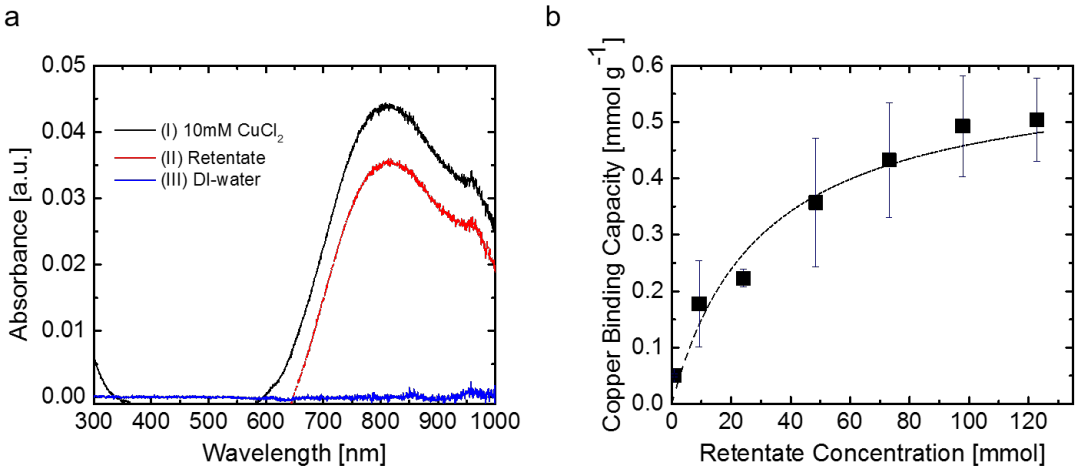

Figure S5. (a) The UV-Vis absorption spectra for (I) 10 mM $CuCl_2$ solution and the (II) adsorption retentate for a 10 mM $CuCl_2$ solution. The wavelength at $\lambda = 830$ nm was used for analysis. The DI-water in (III) was used as the baseline. (b) The equilibrium binding capacity of the membrane is plotted as a function of copper chloride retentate concentration. Herein, the data are shown as black squares and the Langmuir adsorption isotherm is shown as black dotted line. A saturation capacity of 0.60 ± 0.6 mmol g^{-1} of PI-PS-PAA hollow fiber membrane was calculated from Langmuir isotherm.

8. Surface SEM Micrographs and Pore Statistics for PI-PS-PDMA-75 Hollow Fiber Membranes Prepared from Different Dip-coating and SNIPS Conditions

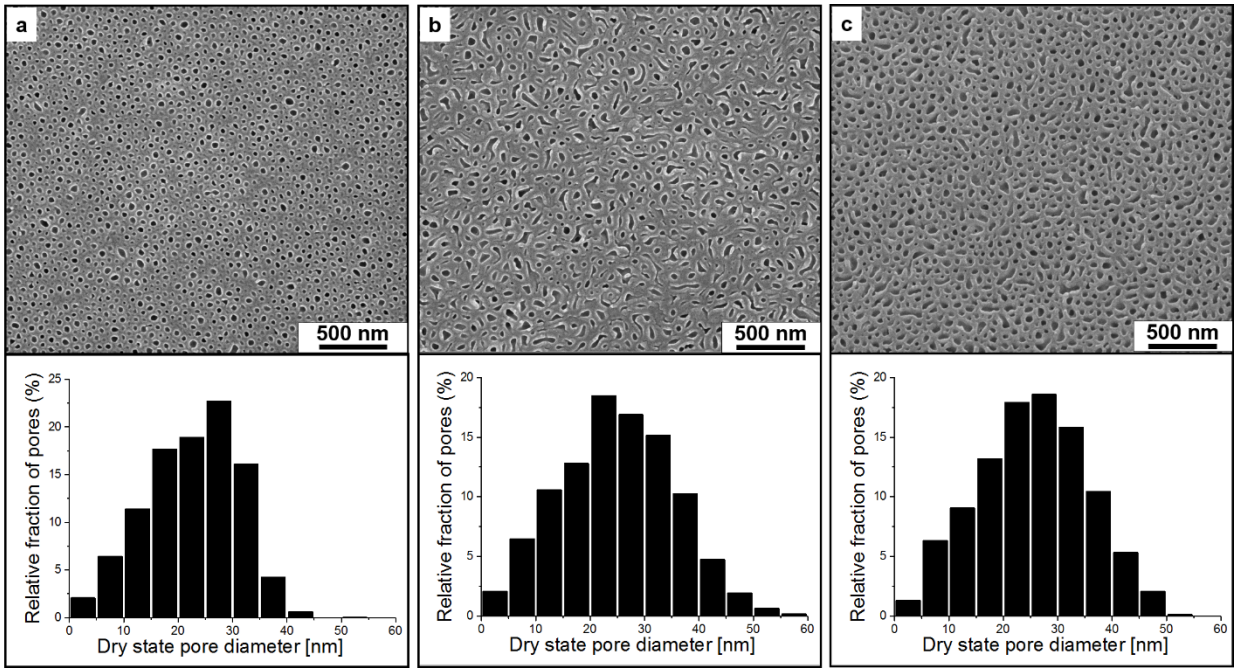

Figure S6. Surface SEM micrographs for the self-assembled surfaces of three membranes prepared from the same polymer solution, but in different dip-coating and evaporation conditions (top row). Their surface pore size distribution, analyzed using the ImageJ software package, are listed in the chart at the bottom of each micrograph (bottom). (a) The 4wt-2.5-45 membrane was prepared with a dip-coating speed of 2.5 mm s^{-1} and a solvent evaporation time of 45 s. This membrane had a dry-state pore diameter of 23 ± 8 nm and a porosity of 2.3×10^{14} pores m^{-2}. (b) The 4wt-2.5-25 membrane was prepared using a dip-coating speed of 2.5 mm s^{-1} and an evaporation time of 25 s. The membrane had a surface pore diameter as 25 ± 10 nm with a porosity of 1×10^{14} pores m^{-2}. (c) The 4wt-5-25 membrane was prepared from a dip-coating speed of 5 mm s^{-1} and an evaporation time of 25 s. This membrane had a dry-state pore diameter as 26 ± 10 nm and a porosity of 1.6×10^{14} pores m^{-2}. Despite the different evaporation time was employed, the three membranes show a similar pore size, and their surface porosity values do not show a significant difference.

9. Non-instantaneous Vitrification Causes an Impermeable Surface Nanostructure, But Does Not Affect Membrane Performance

One minor issue we found on these hollow fiber membranes fabricated from dilute polymer solution and short evaporation times was the co-existence of an impermeable surface with the highly ordered self-assembled nanostructure. These impermeable regions of the surface, which covered only a small fraction of coated surface, may be attributed to non-instantons vitrification process during the precipitation step. However, these were minor, continuous phases, and, as demonstrated by the transport experiments above, the membrane was almost exclusively nanoporous and continuous in nature. In turn, the performance of dual layer hollow fiber was similar to that of the flat-sheet membrane demonstrated in the comparison study.

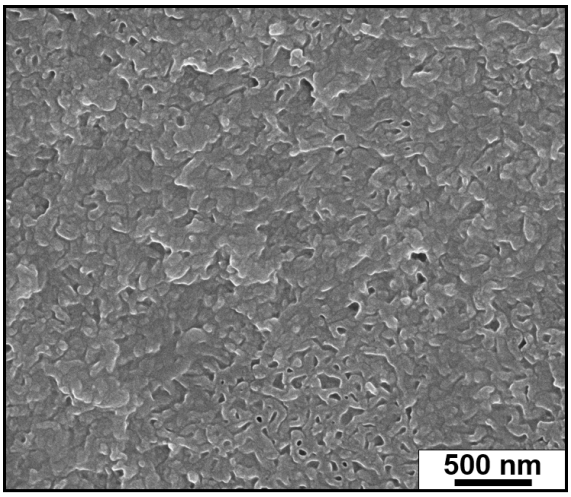

Figure S7. The impermeable surface microstructure was observed during fabrication of PI-PS-PDMA-75 hollow fiber membranes from dilute solution and using a short evaporation time. The presence of impermeable structures on self-assembled surface, which covered only a small fraction of the whole fiber, may be attributed by non-instantons vitrification process during non-solvent phase inversion. The transport experiment of PI-PS-PDMA-75 (4wt-5-25) membrane had a similar performance with PI-PS-PDMA-107 flat-sheet membrane. This result indicates the presence of impermeable microstructure did not impact the performance of membrane.

10. Triblock Polymer Precursor Synthesis Procedures

The synthesis of the polyisoprene-*b*-polystyrene-*b*-poly(*N,N*-dimethylacrylamide) (PI-PS-PDMA) triblock polymer precursors used in this work followed a reversible addition-fragmentation chain transfer (RAFT) polymerization mechanism as detailed previously.[2-4] Using this procedure, isoprene, styrene, and *N,N*-dimethylacrylamide were polymerized sequentially to synthesize the polyisoprene (PI), polystyrene (PS) and poly(*N,N*-dimethylacrylamide) (PDMA) moieties of the PI-PS-PDMA material, respectively. All monomers were purified by passing them through a 5 cm basic alumina (Fisher Scientific) column twice before immediate use. Inhibitor-free, degassed tetrahydrofuran (THF), used as the solvent in the PDMA block addition, was purified by permeating the solvent through an alumina column (Innovative Technology) prior to use. After each step of the polymerization, ^{1}H NMR, which was acquired using a Bruker Avance-III-800 spectrometer, was used to determine the molecular weights of the constituent block polymer domains. These samples were prepared by dissolving ~1% (by weight) solid polymer in deuterated chloroform. The dispersity ($Đ$) values of the PI-PS-PDMA as well as of the PI homopolymer and PI-PS diblock copolymer intermediates were evaluated using size-exclusion chromatography (SEC). A Hewlett-Packard 1260 Infinity series equipped with a Hewlett Packard G1362A refractive index (RI) detector and three PLgel 5 μm MIXED-C columns was used to collect SEC data. The mobile phase flowing at a volumetric flow rate of 1 mL min^{-1} consisted of THF at 40 °C. Polystyrene standards (Agilent) with molecular weights ranging from 1 kg mol^{-1} to 200 kg mol^{-1} were used as the calibration reference.

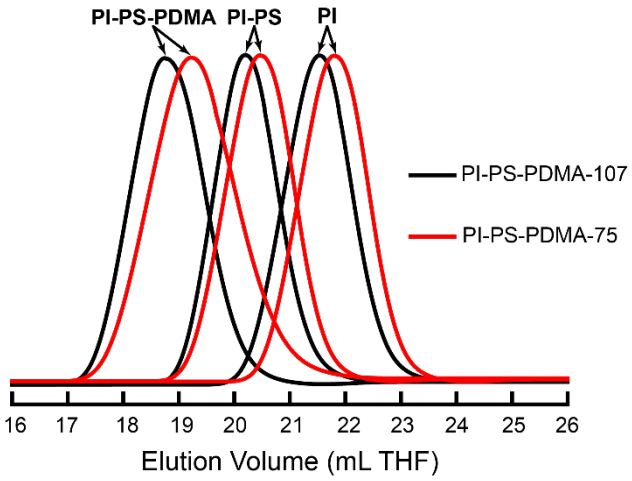

Figure S8. Comparative SEC traces of the RAFT-polymerized PI-PS-PDMA samples with their corresponding PI-PS diblock polymer and PI homopolymer precursor macroinitiating agents used in this study. The PI-PS-PDMA-75 series is shown in red while the PI-PS-PDMA-107 series of materials are shown in black.

References

1. J. L. Weidman, R. A. Mulvenna, B. W. Boudouris and W. A. Phillip, *Langmuir*, 2015, **31**, 11113-11123.

2. D. S. Germack and K. L. Wooley, *J. Polym. Sci., Part A: Polym. Chem.,* 2007, **45**, 4100–4108.

3. R. A. Mulvenna, R. A. Prato, W. A. Phillip and B. W. Boudouris, *Macro. Chem. Phys.*, 2015, **216**, 1831-1840.

4. R. A. Mulvenna, J. L. Weidman, B. Jing, J. A. Pople, Y. Zhu, B. W. Boudouris and W. A. Phillip, *J. Membr. Sci.*, 2014, **470**, 246-256.